ORIGINAL PAPER

Green Synthesis of Triangular ZnO Nanoparticles Using *Azadirachta indica* Leaf Extract and Its Shape Dependency for Significant Antimicrobial Activity: Joint Experimental and Theoretical Investigation

Bhumika K. Sharma[1] · Bijal R. Mehta[1] · Esha V. Shah[1] · Vilas P. Chaudhari[1] · Debesh R. Roy[1] · Sutapa Mondal Roy[2]

Abstract

The present study reports the green synthesis of triangular ZnO nanoparticles (G-ZnO NPs) using *Azadirachta indica* leaves extract, and a shape dependent density functional investigation for ZnO NPs on their antimicrobial activity. The X-ray diffraction (XRD) analysis shows the synthesized G-ZnO NPs are well crystalline in nature and calculated grain size is found to be 60–65 nm. The Fourier transforms infrared spectroscopy (FT-IR) represents that the functional group and capping agents are well attached to the nanoparticles, and the bands located near $500.8 \ cm^{-1}$, $459.07 \ cm^{-1}$ and $418.57 \ cm^{-1}$ represents G-ZnO NPs. Scanning electron microscopy (SEM) and energy dispersive X-ray analysis (EDS) confirmed the presence of the synthesized G-ZnO nanoparticles with an average size range 100–200 nm. The synthesized G-ZnO NPs are found to be in the triangular shape. A detail theoretical investigation under density functional framework shows that our synthesized triangular ZnO nanoparticles are better candidate for biological interactions compared to the prototypical spherical counterpart. The synthesized G-ZnO nanoparticles using *A. indica* leaves extract in triangular shape are found to show significant antimicrobial activity against *Escherichia coli* and *Bacillus subtilis* indicating a better alternative to the typical chemical methods.
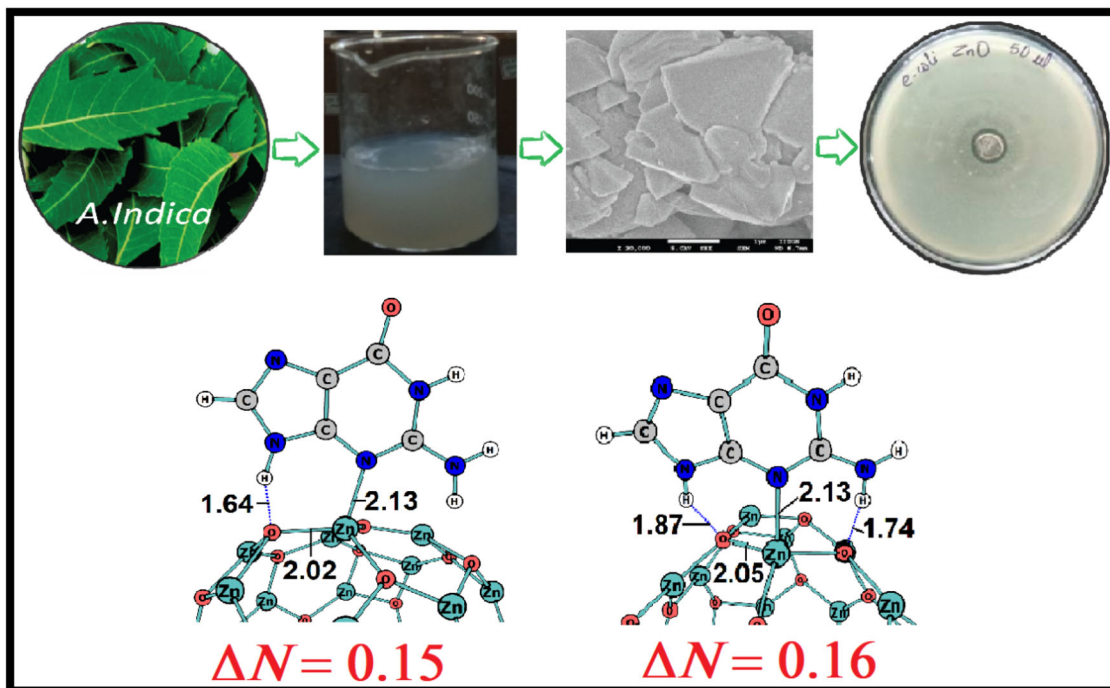
✉ Debesh R. Roy
  drr@phy.svnit.ac.in

✉ Sutapa Mondal Roy
  sutapa.roy@utu.ac.in

1   Materials and Biophysics Group, Department of Physics, Sardar Vallabhbhai National Institute of Technology, Surat 395007, India

2   Present Address: Tarsadia Institute of Chemical Science, Uka Tarsadia University, Maliba Campus, Bardoli, Gujarat 394350, India

Graphic Abstract

Keywords ZnO · Green synthesis · Antimicrobial activity · Shape dependency · Density functional theory (DFT)

Introduction

Nano sized particles have gained exceptional importance due to their various properties and applications in diverse areas including catalysts, biosensors, textile, cancer imaging and therapy etc. [1–4] Metal nanoparticles are noticed to show remarkable properties which is hardly observed in their bulk counterpart. Amongst many metals and non-metals, zinc oxide is known as very versatile material involved in many applications, e.g. solar cells, chemical sensors, photo catalysts, piezoelectric transducers, transparent electrodes [5, 6], ZnO coated fabrics as antibacterial agent [3] etc. It has been observed that the nanoparticles produced by plants are usually more stable, and can be obtained in various shape and size in comparison to those produced by other chemical routes or by microorganisms [7]. Nanoparticles may be synthesized by different methods like precipitation method [8], solvothermal, hydrothermal, sol–gel [9] etc. Chemical synthesis of oxide nanoparticles may lead to the presence of some toxic chemicals on their surface for a possible adverse effect to the relevant medical applications [10]. ZnO nanoparticles have gained immense attention for their versatile properties and useful applications [11–17]. Ong. et al. [11] have reported various

synthesis techniques to synthesize ZnO nanostructures which includes sol–gel precipitation method, hydrothermal, electrochemical, solvothermal, wet-chemical method, flux method, etc. Hasanpoor et al. [12] has synthesized ZnO NPs having needle and flower shape with 50–150 nm in size through microwave assisted hydrothermal method [12]. Samanta and Mishra [13] have reported the formation of nano disc with 300–500 nm size. Laurenti et al. [14] has reported synthesis of nanorod with diameter of 90 nm and length of 564 nm through chemical vapour deposition technique. Anand and Srivastav [15] have reported spherical and cylindrical shaped nanoparticles with sizes 150–200 nm and 50–100 nm, respectively through electrochemical method. Saric et al. [16] has synthesized nanoparticles through solvothermal method using ethanol and without the use of ethanol which forms spherical nanoparticles of 20 nm and 100 nm sizes, respectively. Ghose et al. [17] has reported flakes shape nanoparticles through sonochemical method with 200–400 nm size. Also, in past, a number of researchers have studied biosynthesis of zinc oxide nanoparticles using *Aloe vera*, *Hibiscus subdariffa*, *Corriandrum sativum*, *Ocimum basilicum* L. var, *Purpurascens benth.-Lamiaceae leaf*, *Cinnamomum camphora*, etc. [18–22]. Zinc oxide

nanoparticles also successfully synthesized using *Jacaranda mimosifolia* flowers extract [23] and *Carica papaya* seed extract [24]. Beyond plants extracts, a useful literature resource for biogenic synthesis using algae, fungi, yeast etc. may be found by the work of Bisetty et al. [25].

ZnO NPs synthesized through biological and environmentally benign technology is desirable especially in various bio-medicianl applications including cosmetics, drug carriers and fillers in medical materials [26]. ZnO also finds applications as antimicrobial agent into textiles [27], surface coatings [28] and cellulose fibres [29] to inhibit bacterial growth. ZnO NPs are considered to have antifungal activities as well as potential antimicrobial activities against both Gram-positive and Gram-negative strains of bacteria [10, 30, 31]. Overall, it is understood that the properties and size of the nanoparticles exclusively depends on the respective synthesis routes. Also, the size, morphology, and surface charge play important role in the toxicity of ZnO nanoparticles and their various applications in medical and engineering fields. Many of the metal oxide nanoparticles are noticed to lead to the death of eukaryotic and prokaryotic cells due to their cytotoxicity. The interaction between nanoparticles and cell induces oxidative stress to the cells resulting in the generation of the spontaneous reactive oxygen species (ROS) [32].

In recent times, green synthesis of NPs is attracting researchers due to the advantages of its simplicity, inexpensiveness and non-toxicity. In the present work a green method is used for the synthesis of ZnO nanoparticles (G-ZnO) using *Azadirachta indica* leaves extract. The obtained plant leaf extract and NPs were characterized and confirmed by Fourier transform infrared spectroscopy (FTIR), X-ray diffraction (XRD) technique, Scanning electron microscopy (SEM) images and Energy dispersive X-ray analysis (EDS). A critical theoretical investigation has also been carried out to understand the shape (triangular and spherical) dependent biological activities of ZnO nanoparticles against *Escherichia coli*.

Materials and Method

Plant Collection

Fresh and healthy leaves of *Azadirachta indica* were collected from S.V. National Institute of Technology, Surat campus (Gujarat). The leaves sample collected were intermediate stage, i.e., between juvenile and adult.

Preparation of *Azadirachta indica* Leaf Extract

To prepare the leaf extract of *A. Indica* leaves (50 g) were washed thoroughly with running water then with Deionized water (DI water), dried and are finely chopped [33]. The 100 g of finely chopped leaves are then allowed to boil in 500 ml of de-ionized water in a 1000 ml of Erlenmeyer flask and the amount is reduced to 70% and then cooled down to room temperature. The resulting extract is then filtered using Whatman Filter paper of pore size 0.2 μm to remove any solid particles present in extract. The filtrate is then collected and stored at 4 °C for the synthesis of G-ZnO NPs.

Green Synthesis of ZnO NPs

Zinc nitrate hexahydrate $(Zn(NO_3)_2 \cdot 6H_2O)$ of analytical amount 184.3 g was dissolved in 100 ml of DI water [34], after complete dissolution of mixture, 20 ml of prepared *A. indica* leaf extracts was added to the solution with vigorous stirring at 100 °C for 1 h. The solution color changes from green to yellowish green. The solution is then collected in quartz crucible and calcined at 400 °C in muffle furnace for 2 h resulted with the formation of off- white colored powder. The formed G-ZnO NPs were then grinded in mortar pestle and collected for further characterization.

Characterizations of ZnO NPs

X-ray Diffraction (XRD)

The elementary analysis of synthesized material was carried out using X′ Pert Pro A Analytical X-ray diffractometer using Cu Kα radiation in the range of 30–80° at 3 kW, and was used for phase identity and crystalline size of NPs.

FTIR Spectroscopy

FTIR spectra for both *A. indica* leaf extract and ZnO NPs were obtained from SHIMADZU FTIR-8400S Fourier Transform InfraRed Spectrophotometer. To take the FTIR spectra of both the samples, standard KBr-pellet method of sample preparations was followed. The FTIR spectra of both the leaf extract and nanoparticles were taken in the region of 4000–400 cm^{-1} and are presented in Figs. 2 and 3, respectively. The spectrometer was continuously purged with dry nitrogen. Both the samples were scanned under the same conditions.

Scanning Electron Microscopy (SEM)

The surface morphology of G-ZnO nanoparticles as synthesized by green route were examined by means of Field Emission Scanning Electron Microscope (JEOL JSM76007 @ IITGN) at 5 kV voltage.

Table 1 Antibacterial activity of G-ZnO nanoparticles evaluated in terms of zone of inhibition (ZOI, mm) against *E. coli* and *B. subtilis* at different concentration (in μl). The borer diameter (B_d) has an average value of 8 mm

Bacteria	Concentration of G-ZnO NPs (μl)	ZOI′ (incl. B_d) (mm)	ZOI = ZOI′-B_d (mm)
E. coli	50	11.0 ± 0.25	3.0 ± 0.25
	75	12.5 ± 0.25	4.5 ± 0.25
B. subtilis	50	13.0 ± 0.25	5.0 ± 0.25
	75	14.5 ± 0.25	6.5 ± 0.25
	100	15.5 ± 0.25	7.5 ± 0.25

Energy Dispersive Spectroscopy (EDS)

The elementary analysis of the nanoparticles is performed using Energy Dispersive Spectroscopy (OXFORD, MODEL INCA ENERGY 250 EDS).

Antibacterial Study

The antibacterial activity was performed against Gram-negative bacterial strain *Escherichia coli* (ATCC 25922) and Gram-positive strain *Bacillus subtilis* (ATCC 23857) by agar well diffusion method [35, 36]. Nutrient agar plates using Luria Broth (LB) and Luria Agar (LA) and matured broth culture of *E. coli* and *B. subtilis* was prepared. The bacterial culture of 200 μl was mixed with top agar and is poured over the base agar. After solidification of the agar plates, wells were made carefully using cup borer of diameter of 8 mm (B_d). The nanoparticles were well-dispersed in sterile water. The wells of the Agar plates were filled with different concentration of G-ZnO NPs as per the requirement of the experiment. Finally, the plates were incubated at 37 °C for 24 h. The zone of inhibition (ZOI) values were measured after the incubation period. All of these results of antibacterial activities in the form of ZOIs are presented in Figs. 6 and 7, and tabulated in Table 1.

Theoretical Methods

In order to understand the interactions between nanoparticles (ZnO) and biosystem (*E. coli*), we have searched for the representative nanoclusters for ZnO with spherical and triangular shape. As a result of critical search for suitable nanoclusters with spherical and triangular shape and comparable average sizes, we have obtained spherical $(ZnO)_{24}$ and triangular $(ZnO)_{25}$ nanoclusters of average size about 1 nm for investigation to meet the requirement to understand the experimental observations. On the other hand, we have considered the nuclic acids (DNA and RNA) base Guanine as the model biosystem for *E. coli*, since Guanine is reported to possess the maximum electronegativity compared to all other nuclic acid bases Adenine,

Cytosine, Thymine and Uracil [37]. The geometry of Guanine as well as its complex with considered spherical and triangular nanoclusters are also optimized to gain more insight on their interactions. The charge transfer (ΔN) and energy transfer (ΔE) between the spherical and triangular ZnO nanoclusters and the Guanine is also computed to understand the shape (spherical and triangular) dependent antibacterial activities of ZnO nanoparticles. The geometries of all the zinc oxide clusters and their Guanine complexes, *A. indica* leaf extract compounds and their Zn^{2+} complexes are optimized under the framework of Density Functional Theory (DFT) [38] by utilizing GAUSSIAN 09 [39] suits of programs. A molecular orbital method is approached using linear combination of atomic orbitals (LCAO) to examine the electronic structure. A very popular hybrid functional, namely, Becke 3- parameter exchange and Lee–Yang–Parr correlation (B3LYP) functional [40] is employed in the Hamiltonian. A standard basis set, namely, LANL2DZ (Los Alamos ECP plus D.Z.) is considered which includes a scalar relativistic correction [41, 42]. In order to examine the effect of Grimme dispersion correction (D3 parameter) [43, 44] in the basis set, we have also calculated DFT-D3 calculations for all the system and compared the respective electronic properties.

The following are the various reactivity parameters calculated to determine charge (ΔN) and energy transfers (ΔE) between nanoparticles and biosystem. The chemical potential (μ) [45] and chemical hardness (η) [46] are defined as the first and second derivative of total electronic energy (E) in respect to the total number of electrons (N), at a constant external potential $v(r)$:

$$\mu = \left[\frac{\partial E}{\partial N} \right]_{v(\vec{r})} \qquad (1)$$

$$\eta = \frac{1}{2} \left[\frac{\partial^2 E}{\partial N^2} \right]_{v(\vec{r})} = \frac{1}{2} \left[\frac{\partial \mu}{\partial N} \right]_{v(\vec{r})} \qquad (2)$$

The electronegativity (χ) can be defined as the negative of chemical potential (μ) as [45]:
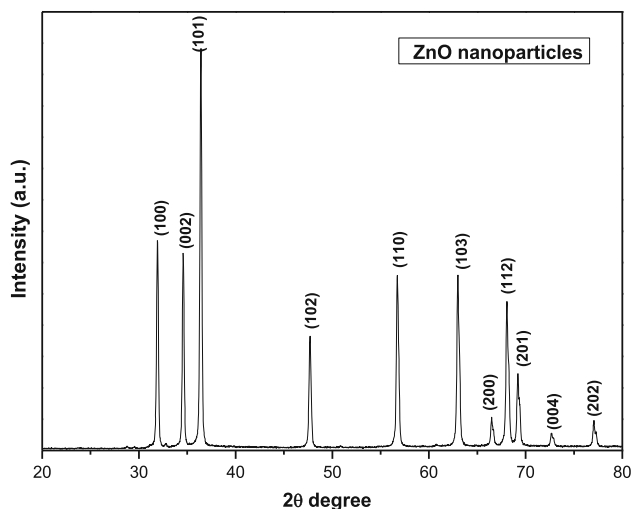
Fig. 1 XRD pattern for green synthesized G-ZnO nanoparticles

$$\chi = -\mu = -\left[\frac{\partial E}{\partial N}\right]_{v(\vec{r})} \tag{3}$$

Parr et al. [47] have defined electrophilcity index (ω) as the measure of maximal transfer of electrons from a donor to acceptor as follows:

$$\omega = \frac{\mu^2}{2\eta} = \frac{\chi^2}{2\eta} \tag{4}$$

which can be considered as a measure of electrophilicity of the ligand.

Parr and Pearson [48] proposed an expression to measure the amount of charge transfer (ΔN) and the energy transfer (ΔE) from a molecule A towards another molecule B as follows:

$$\Delta N = \frac{\chi_A - \chi_B}{2(\eta_A + \eta_B)} \tag{5}$$

$$\Delta E = \frac{(\chi_A - \chi_B)^2}{4(\eta_A + \eta_B)} \tag{6}$$

where χ and η presents electronegativity and chemical hardness, respectively. In the present work, spherical and triangular nanoclusters are considered to be system **A** whereas Guanine (model biomolecule) is chosen as system **B**.

Results and Discussions

X-Ray Diffraction (XRD)

The phase identity and crystalline size of NPs were characterized using X'Pert Pro A Analytical X-ray diffractometer using Cu Kα radiation in the range of 30–80° at 3 kW.

Figure 1 shows the XRD diffraction peaks at 2θ of 31.96, 34.54, 36.36, 47.76, 56.66, 63.02, 66.56, 68.06, 69.24, 72.68 and 77.68 degrees which were assigned to the 110, 002, 101, 102, 110, 103, 200, 112, 201, 004, and 202 planes respectively [49]. The narrow and strong diffraction peaks indicate the well crystalline nature of zinc oxide. The Scherrer's formula was used to calculate the particle sizes and was observed and calculated particle sizes belongs within the size range of 60–65 nm.

XRD study confirmed the presence of even smaller particles than that observed in SEM examination as reported in the Sect. 3.3. The agglomeration of smaller nanoparticles occurred due to the fact that we are dealing with biological material and presence of the moisture in atmosphere.

Fourier Transform Infrared Spectroscopy (FTIR)

The results were further analyzed using FTIR analyses where it showed the shift and differences in peak area. Figure 2a, b show the FTIR spectra attributed to *A. indica* leaves extract and green synthesized G-ZnO NPs, respectively. The FTIR spectrum of *A. indica* leaves extract and green synthesized G-ZnO NPs were recorded in the range of 400–4000 cm^{-1}. The FTIR spectra as represented by Fig. 2a, confirms the existance of several chemical moieties (functional groups) coming from the phytochemicals as present in the *A. indica* leaves, whereas Fig. 2b confirms the existance of ZnO NPs as well as the phytochemicals, as discussed below.

The FTIR spectrum of *A. indica* leaves extract in Fig. 2a shows the presence of some significant bands viz. 3399.52 cm^{-1} (O–H stretching vibration of polyphenols like gallic acid) [50], 1719.42 cm^{-1}, 1119.60 cm^{-1} and 1033.77 cm^{-1} (stretching frequency of C=O and C−O bonds of ascorbate, nimbin, hydroxyazadiradione) [51, 52], 2964.39 cm^{-1} and 2928.71 cm^{-1} (C−H stretching frequencies due to the organic phytochemicals), 1629.74 cm^{-1} and 1599.84 cm^{-1} (stretching and bending vibrations of C=C of ascorbate, nimbin, hydroxyazadiradione etc.) [53–56]. Figure 2b shows the FTIR spectra of green synthesized G-ZnO NPs. Upon formation of the nanoparticles, most of the significant stretching frequencies of bands as mentioned in Fig. 2a are found to be either shifted or significantly lowered in intensity. The substantial disappearance of the FTIR bands due to the stretching vibrations of O–H group, C=O, C−O and C=C bonds have been observed in case of the FTIR spectrum of G-ZnO NPs. At the same time shifted bands with very low intensity are also marked e.g. O–H group stretching (around

Fig. 2 FTIR spectra of **a** *A. indica* leaves extract and **b** G-ZnO NPs using *A. indica*
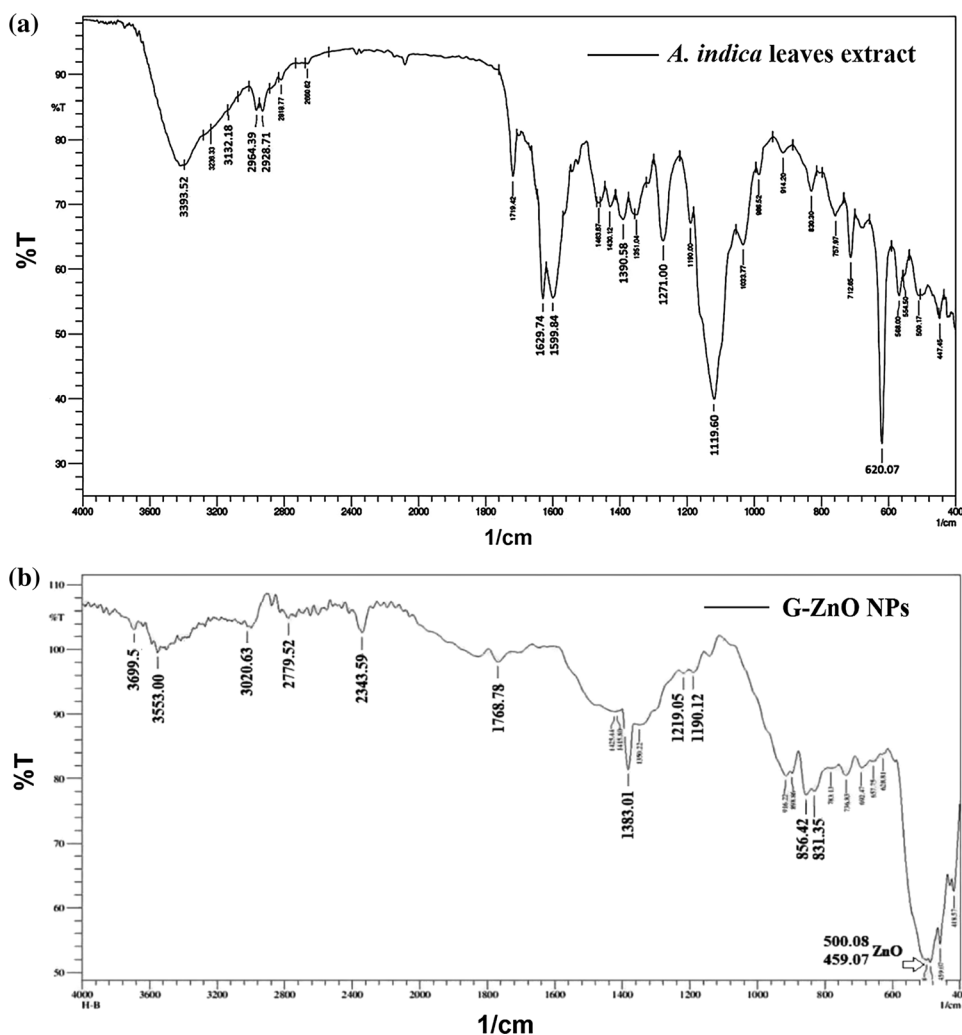
3553.00 cm^{-1} and 3020.63 cm^{-1}), –C–O acid stretching (1383.01 cm^{-1}), aldehyde stretching (1768.78 cm^{-1}) etc.

The new bands at around 2300–2900 cm^{-1} can be attributed to the C=C–H stretching, O=C–H stretching and C≡C stretching. This is consistent with the reduction of the phytoconstituents of the neem leaf extracts to form the oxide nanoparticles. These findings indicate the involvement of several of these functional groups, e.g. phenolic group, carbonyl group, carboxylate group, ether group etc. in the formation and stabilization of the ZnO nanomaterials. Moreover, in the Fig. 2b, the bands located near 500.8 cm^{-1}, 459.07 cm^{-1} and 418.57 cm^{-1} are due to the standard stretching vibration of Zn–O bond [57, 58], which confirms the existence of our green synthesized zinc oxide nanoparticles, and similar characteristics also reported by Yuvakkumar et al. [59] in past.

Scanning Electron Microcopy (SEM)

Th Field Emission Scanning electron microcopy (FE-SEM) images and size distribution of G-ZnO nanoparticles are shown in Fig. 3. The figures show the surface morphology of synthesized nanoparticles, indicating that G-ZnO nanoparticles are relatively triangular in shape. It was also shown that the particles were found in the average range of 100–200 nm and appeared to be agglomerated on to the surface due to the electrostatic interactions between the bio-organic capping molecules bound to the G-ZnO nanoparticles. It may be noted that although most of the particles contains smaller sizes ranging between 50 and 300 nm (Fig. 3b), providing average particle size as 100–200 nm, the distinct triangular shape is observed in the order of 1 μm. The agglomeration of smaller nanoparticles occurs due to the fact that the preparation of the nanoparticles deals with biological material with the presence of moisture in atmosphere. *A. indica* constitutes of number of complex active ingredients like azadirachtin,

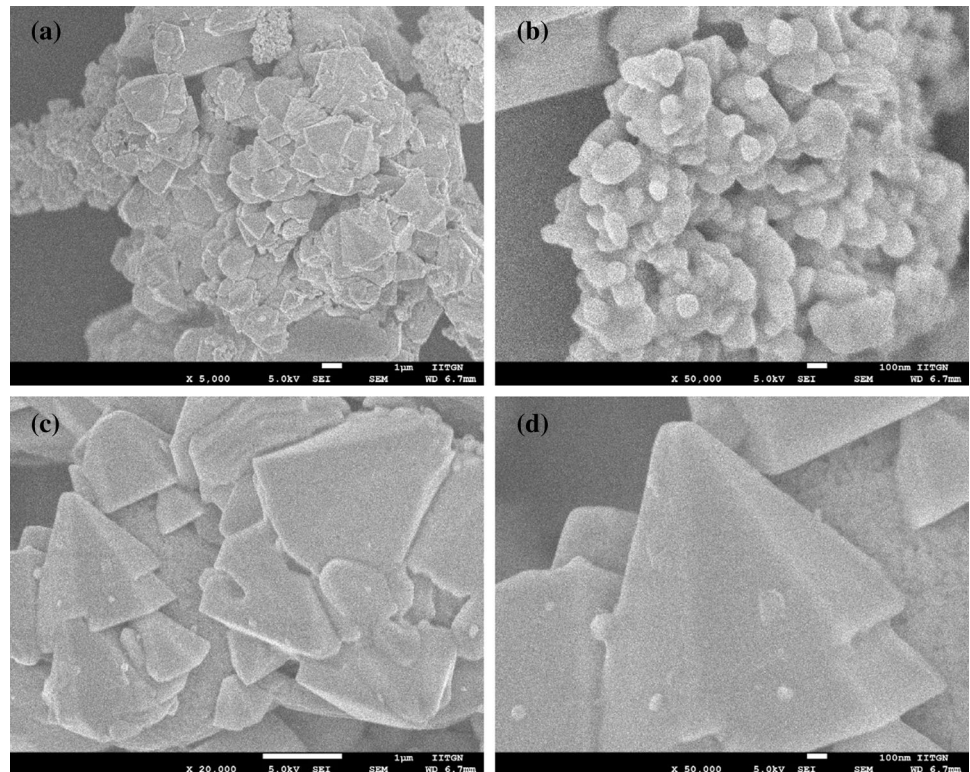**Fig. 3** SEM images of green synthesized ZnO (G-ZnO) NPs

Fig. 4 EDS image and elemental plot of green synthesized ZnO (G-ZnO) NPs
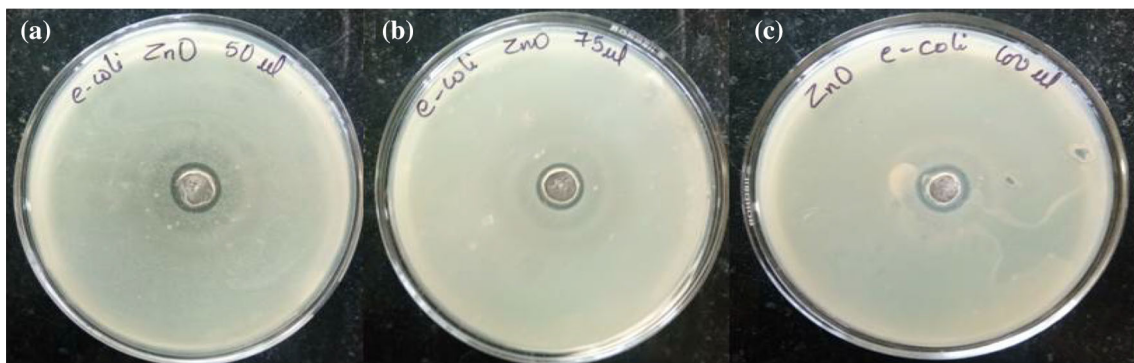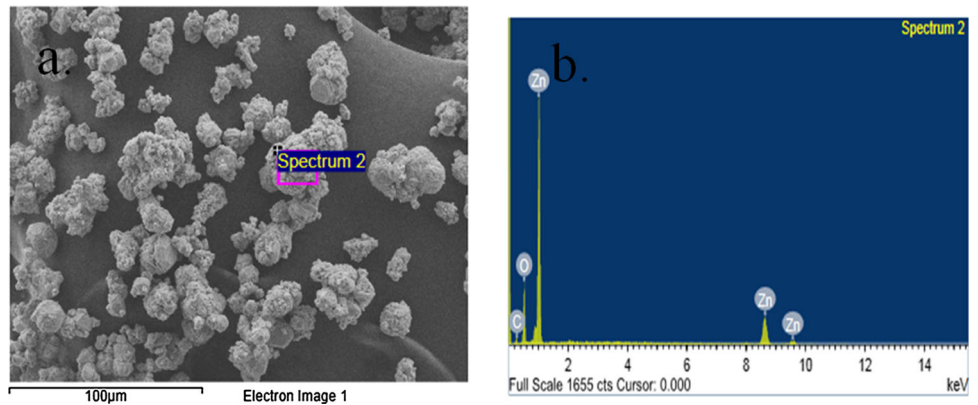

Fig. 5 Images of colonies of *E. coli* on Agar diffusion plate in the presence of G-ZnO NPs at different concentrations: **a** 50 μl, **b** 75 μl and **c** 100 μl
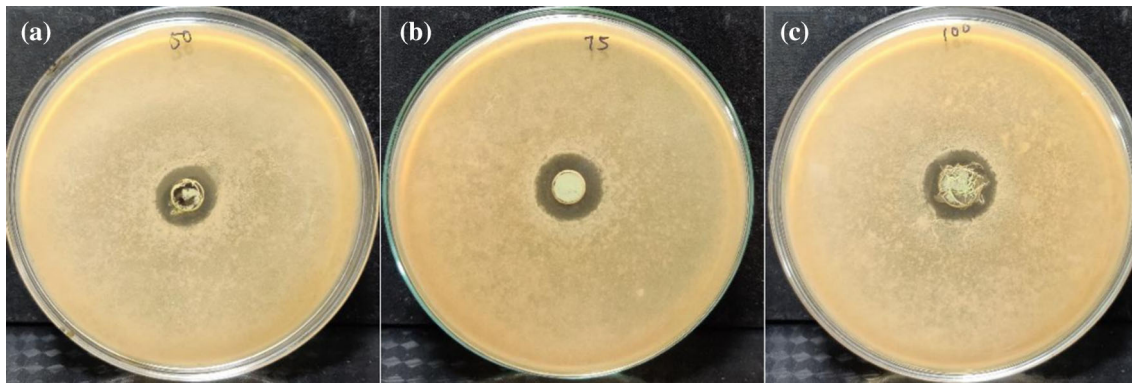
Fig. 6 Images of colonies of *B. subtilis* on Agar diffusion plate in the presence of G-ZnO NPs at different concentrations: **a** 50 μl, **b** 75 μl and **c** 100 μl

nimbolinin, nimbin, nimbidin, nimbidol, salannin, hydroxyazadiradione, gallic acid, azadiradione, 6-deacetylnimbinene, 3-deacetylsalannin, 2,3-dihydronimbolide etc. [60–66] which help in reducing the nanoparticles by breaking of molecules. It also be noted that *A. indica* plant extract act as a stabilizing agent with formation of coating on the surface of nanoparticles during the biosynthesis process.

Energy Dispersive Spectroscopy (EDS)

The EDS analysis shows sharp and narrow peaks for the Zinc (Zn) and Oxide (O) with their confirmation in the NPs, and elemental mapping for green synthesized G-ZnO nanoparticles is presented in Fig. 4.

Antibacterial Activity

The antibacterial activity of green synthesized ZnO nanoparticles performed against standard clinical bacterial strains Gram-negative *E. coli* and Gram-positive *B. subtilis* are demonstrated in Figs. 5 and 6, respectively. The antibacterial activity is evaluated by agar-well diffusion method by measuring the relevant zone of inhibition (ZOI). The bacterial strains were sub cultured using Luria Bertani (LB) broth and were incubated at 37 °C for 24 h. A well of 8 mm diameter, i.e. borer diameter (B_d) was punched into Luria broth agar having microorganisms. Certain quantity of nanoparticles and one milliliter (mL) autoclaved double distilled water (as control) were inoculated into the well. The well is diffused with G-ZnO NPs at the concentrations of 50 μl, 75 μl and 100 μl. It is observed in the lawn for the growth of microorganism, G-ZnO NPs shows effective antibacterial activity to both the *E. coli* and *B. subtilis*. It is

Table 2 Antibacterial activity of G-ZnO nanoparticles through chemical, physical and green synthesis methods in terms of size of the nanoparticles and ZOI′ (including borar diameter) against Gram-negative *E. coli* and Gram-positive *B. subtilis*

Sl	Synthesis	Methods	Size (nm) (Shape)	NPs conc	ZOI′ (mm)	Organism	Refs
1	Chemical	In situ formation of hydrogel matrix	10–20 (hydrogel matrix)	5 cm disc of hydrogel	14	*E. coli*	[71]
2	Chemical	Sol–gel	5–50 (thorn)	50 μl	7	*E. coli*	[70]
3	Chemical	Sol–gel	30–50 nm (hexagonal)	0.938 mg/mL	15	*B. subtilis*	[72]
4	Physical	Mechano-chemical	20–40 (spherical)	500 μg/disc	22	*E. coli*	[73]
5	Physical	Pulsed laser ablation	50–80 (hexagon)	1 mg/cm^2 of fabric	20	*E. coli*	[74]
6	Green	*R. graveolens*	20–30 (spherical)	40 μl	1.67	*E. coli*	[71]
7	Green	*S. nigrum*	29.79 (quasi spherical)	20 μl	7	*E. coli*	[75]
8	Green	*A. indica*	40 (spherical)	50 μg/ml	12.6	*E. coli*	[76]
9	Green	*A. indica*	20–45 (wurtzite)	50 μg/ml	13.0	*B. subtilis*	[69]
10	Green	*Goat faecal matter*	28.5 (spongy)	100 μg/ml	8.46	*B. subtilis*	[77]
11	Green	*A. indica*	100–200 (triangular)	100 μl	13.8	*E. coli*	Present work

observed that as the concentration of NPs increases, the zone of inhibition also increases (Table 1). According to Sunada et al. [67], the interaction of G-ZnO NPs with microorganisms is due to the release of oxygen species on the surface of ZnO NPs which causes fatal damage on microorganisms. The released O species react with hydrogen ions to form H_2O_2 depending on the surface area of the ZnO nanoparticles. The H_2O_2 further penetrate the cell membrane and kills cells, resulting in a higher antibacterial activity [68].

It may be noted that ZnO NPs synthesized using *A. Indica* in the range of 100–200 nm show good antibacterial activity against Gram-negative *E. coli* at 50 μl concentrations in terms of ZOI as 11.0 ± 0.25 mm, and the same is increases with the increase of nanoparticles concentrations. It's also interesting to note from Table 1, Figs. 5 and 6 that ZnO NPs shows better activity against *B. subtilis* (ZOI 11 ± 0.25 mm at 50 μl) in comparison to the *E. coli*, and similar observation was also noted by Elumalai and Velmurugan in past [69]. A number of attempts have been made by the researchers to synthesize ZnO nanoparticles through various chemical, physical and green synthesis methods, due to its various useful applications and versatile properties. Table 2 presents comparative literature information on the antibacterial study of ZnO NPs on *E. coli*

and *B. subtilis* with different chemical, physical and green synthesis methods along with the present work. It may be noted that G-ZnO synthesized using *A. indica* shows good antibacterial activity. The unique feature of G-ZnO NPs is its triangular shape which gives active site for interaction with biomolecules and microorganisms shows good activity even with a large size (100–200 nm). Khan et al. [70] has synthesized thorn shape CuO NPs (size 5–50 nm) by Sol–gel method and its antibacterial activity was found to be in terms of ZOI as 07 mm at 50 μl of NPs. Similarly, Lingaraju et al. [71] has used *Rutagraveolens stem extract* for synthesis of CuO NPs (of size 20–30 nm) and its antibacterial study in terms of ZOI as 1.67 mm at 40 μl [71]. In present work, ZnO NPs synthesized using *A. Indica* leaf extract may be a preferable synthesis route in eco-friendly way and their possible medical applications.

Theoretical Studies

In the present work, we report green synthesis of triangular shaped ZnO nanoparticles using *A. indica* leaf extracts. Several studies, involving the techniques e.g. LC–MS, HPLC–MS, ESI–MS, FTIR, ATR-FTIR etc. regarding the constituents present in the polar-solvent-extract of *A. indica* leaves, have corroborated the existence of
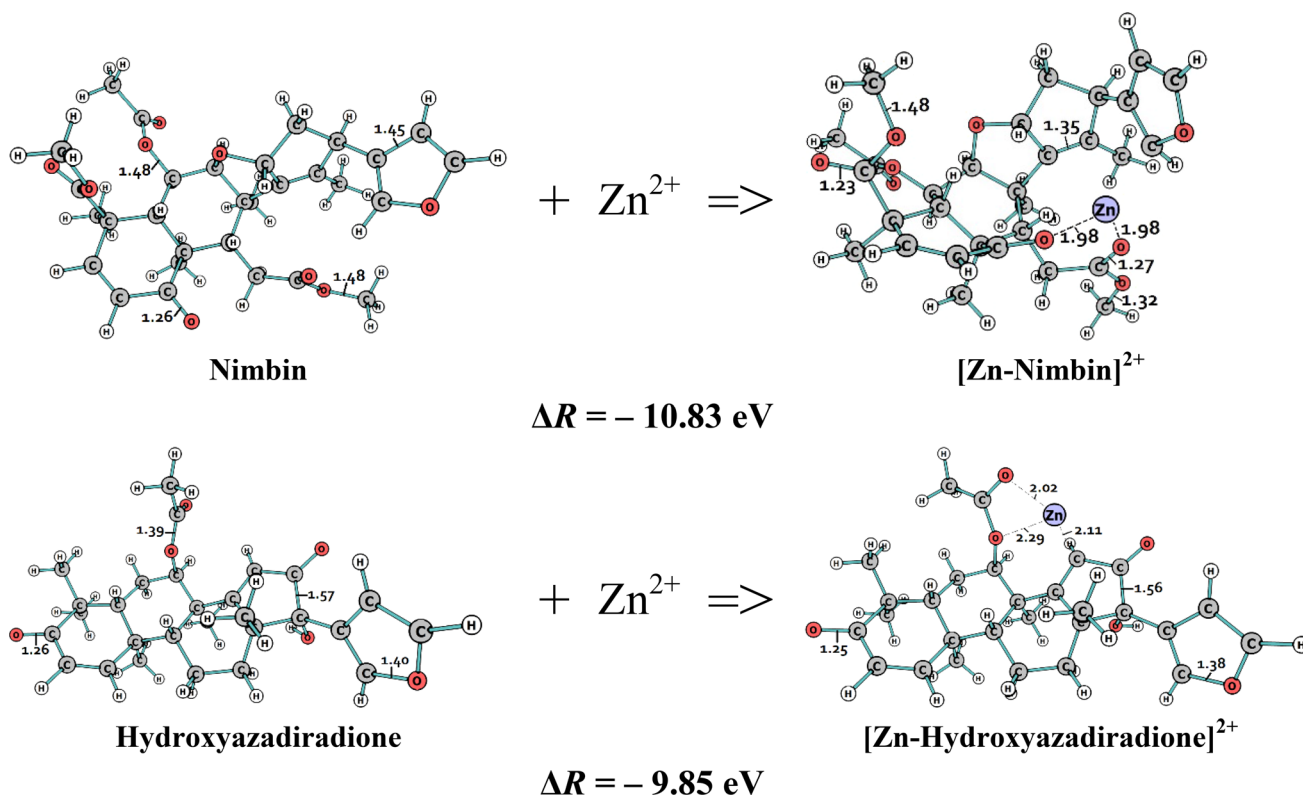

Fig. 7 Optimized structures of Nimbin and Hydroxyazadiradione molecules and their Zn^{2+} complexes along with respective reaction energies (ΔR)

Table 3 Total electronic energy (E), ionization potential (IP) and electrophilicity (ω) of Zn^{2+}, nimbin, hydroxyazadiradione and their complexes along with their reaction energies (ΔR)

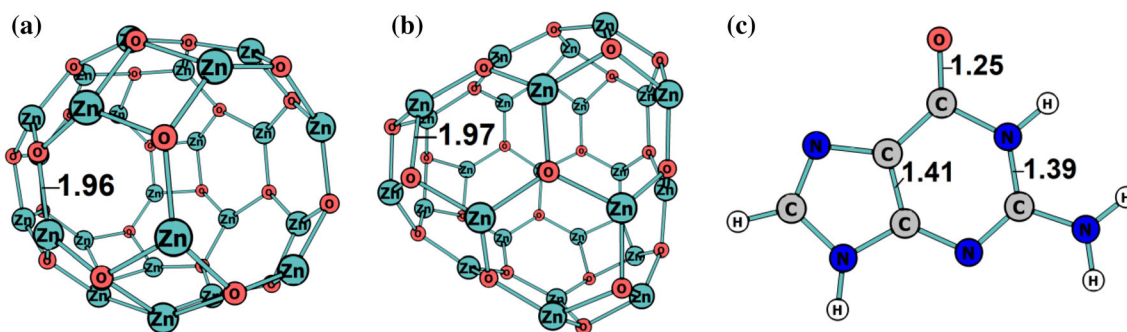| Systems	E (au)[a]	IP (eV)	ω (eV)	ΔR (eV)
Zn^{2+}	− 64.63	36.17	48.46	–
Nimbin	− 1841.56	6.15	4.21	–
[Zn-Nimbin]$^{2+}$	− 1906.62	12.12	36.17	− 11.84
Hydroxyazadiradione	− 1538.50	6.39	4.31	–
[Zn-Hydroxyazadiradione]$^{2+}$	− 1603.49	11.45	190.22	-9.85
Gallic acid	− 645.58	16.72	149.84	–
S1	− 494.614	7.44	0.24	–
S2	− 495.963	7.04	0.14	–

[a] 1 au = 27.21 eV

Fig. 8 The optimized geometries of **a** (ZnO)$_{24}$ (spherical), **b** (ZnO)$_{25}$(triangular) nanoparticles and **c** Guanine nucleic acid base

polyphenols, phenolic acids, flavonoids, terpenoids etc. out of which, nimbin, hydroxyazadiradione, gallic acid, salannin, azadiradione, 6-deacetylnimbinene, 3-deacetyl-salannin, 2,3-dihydronimbolide are important [61–66]. Since the presence of nimbin, hydroxyazadiradione, and gallic acid are considered to be significantly high in the aqueous extract of neem leaves, the theoretical studies have been performed using these three important phytochemicals.

The structures, total electronic energy (E), ionization potential (IP) and electrophilicity (ω) of Zn^{2+}, nimbin, hydroxyazadiradione and their complexes, viz. [Zn-Nimbin]$^{2+}$ and [Zn-Hydroxyazadiradione]$^{2+}$ are reported in Fig. 7 and Table 3. The reaction energies (ΔR) to form those complexes are also provided in the table. It may be noted that the negative reaction energies for both the Zn^{2+} and *A. indica* leaf extracts complexation process indicate their exothermic nature and therefore thermodynamically favorable. Also, larger IP of the zinc complexes, viz. [Zn-Nimbin]$^{2+}$ (12.12 eV) and [Zn-Hydroxyazadiradione]$^{2+}$ (11.45 eV) in comparison to their respective molecules indicates better stability of the complexes. The large enhancement of electrophilicity values in the complexes imply that these extract agents have high reactivity towards zinc, which certainly helps in formation of the ZnO nanoparticles via these metal-complex intermediates. The favorable energy values for the structures derived from

gallic acid viz. S1 and S2 [Scheme 1, Fig. 10], also point out to the fact that formation of these structures are quite possible as the byproduct of the main synthesis of $Zn(OH)_2$, which in turn gives the ZnO nanoparticles.

It may be noted that ZnO nanoparticles are reported mostly with the of spherical shape [73–77], whereas triangular shape is hardly reported. It certainly motivated us for investigating the antibacterial efficacy of triangular ZnO and compare the same with the prototypical spherical shaped ZnO nanoparticles. Aoordingly, we have carried out a detail and representative calculation on the comparative shape dependent bio-activities for spherical and triangular ZnO nanoparticles against any microorganism (e.g. *E. coli*, *B. subtilis* etc.) through consideration of model biosystem. The spherical (ZnO)$_{24}$ and triangular (ZnO)$_{25}$ nanoclusters of average size about 1 nm are considered as representatives for respective nanoparticles. It is understood that since nanoparticles are most commonly interacting with nucleic acids (DNA and RNA) bases, we have chosen the highest electronegative nucleic acid base Guanine as the model biosystem for *E. coli* or *B. subtilis*.

Figure 8 presents the optimized geometries of spherical (ZnO)$_{24}$ and triangular (ZnO)$_{25}$ nanoparticles, and the Guanine nucleic acid base. Both the representative spherical and triangular ZnO nanoclusters are considered with comparable average size about 1 nm to meet the
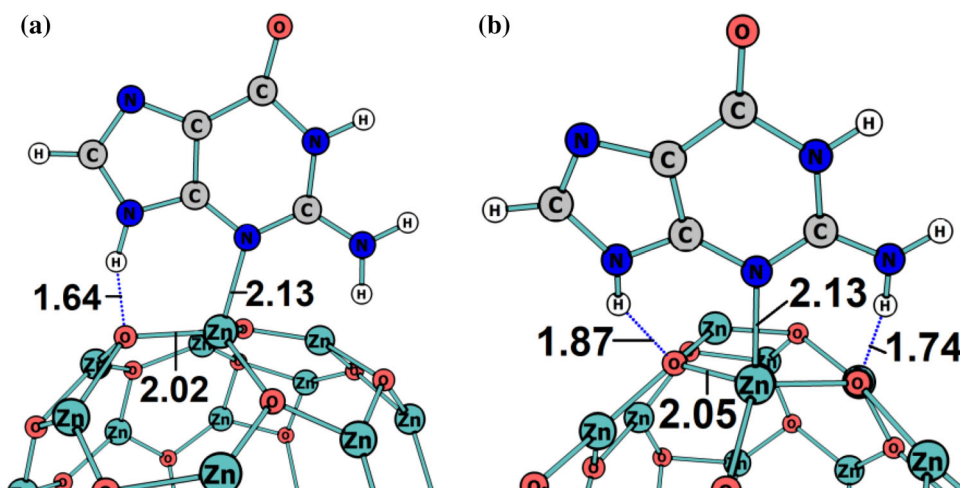
Table 4 Total electronic energy (Total E), chemical hardness (η), electronegativity (χ), electrophilicity (ω), electron transfer (ΔN) and energy transfer (ΔE) with Guanine for the modeled $(ZnO)_{24}$ (spherical) and $(ZnO)_{25}$ (triangular) zinc oxide nanoparticles. The calculationas are carried out using LANL2DZ (L2) and DFT-D3 (D3) basis sets

Systems	Total E (au)		η (eV)		χ (eV)		ω (eV)		ΔN (eV)		ΔE (eV)	
	L2[a]	D3[b]	L2	D3	L2	D3	L2	D3	L2	D3	L2	D3
Guanine	− 542.46	− 542.47	2.67	2.67	3.33	3.33	2.08	2.07	–	–	–	-
$(ZnO)_{24}$: Sph	− 3381.61	− 3381.79	2.00	1.99	4.72	4.69	5.57	5.51	0.149	0.146	0.103	0.099
$(ZnO)_{25}$: Tri	− 3522.51	− 3522.71	1.89	1.88	4.75	4.72	5.96	5.89	0.155	0.152	0.110	0.105

[a]L2: LANL2DZ

[b]D3: DFT-D3

Fig. 9 The optimized geometries of **a** $(ZnO)_{24}$ (spherical)–Guanine and **b** $(ZnO)_{25}$(triangular)–Guanine interactions

requirement of a representative nanoparticle to understand experimental observations.

The Table 4 provides the total electronic energies, chemical hardness, electronegativity and electrophilicity values of Guanine, $(ZnO)_{24}$ and $(ZnO)_{25}$. The electron and energy transfer values of spherical $(ZnO)_{24}$ and triangular $(ZnO)_{25}$ nanoclusters with model biosystem Guanine is also reported. It may be noted from the Table 4 that higher electrophilicity value of triangular $(ZnO)_{25}$ (5.96 eV) in comparison to its spherical counterpart indicate its more reactive nature which may facilitate better interaction to the biosystem. Also, larger electron transfer (ΔN) and energy transfer (ΔE) of triangular $(ZnO)_{25}$ with model biosystem Guanine confirms its potency over the spherical particle for better biological activity facilitated with larger electronic interactions. A similar obserbation is also reported by our group in recent past for the green synthesized rock-salt magnesium oxide nanoparticles (MgO NPs) over its spherical counterpart, at the same level of calculations [78]. It also may be noted that the incorporation of Grimme dispersion effect (DFT-D3) in the considered systems also shows similar qualitative trends and therefore

confirms the better interactions (in terms of ω, ΔN and ΔE) for the triangular ZnO nanoparticle over its spherical counterpart.

Further, in order to investigate the actual interaction of the considered spherical and triangular nanoclusters with Guanine, we have carried out large scale simulations. The relaxed complexes of spherical $(ZnO)_{24}$-Guanine and triangular $(ZnO)_{25}$-Guanine are presented in Fig. 9. It may be noted from the figure that Guanine shows stronger adsorption on the triangular nanocluster (Fig. 9b) with two hydrogen bond interactions (O….H) over its spherical counterpart (one O….H bond, Fig. 9a) in addition to the covalent Zn-N bond. The present theoretical study clearly indicates that the triangular ZnO nanoparticles as observed in our present experiment are more reactive and biologically active in comparison to prototypical spherical ZnO nanoparticles.

Proposed Mechanism

Several studies, involving the techniques e.g. LC–MS, HPLC–MS, ESI–MS, FTIR, ATR-FTIR etc. regarding the constituents present in the polar-solvent-extract of *A. indica* leaves, have corroborated the existence of polyphenols, phenolic acids, flavonoids, terpenoids etc. out of which, nimbin, hydroxyazadiradione, gallic acid, salannin, azadiradione, 6-deacetylnimbinene, 3-deacetyl-salannin, 2,3-dihydronimbolide are important [61–66]. Since the presence of nimbin, hydroxyazadiradione, and gallic acid are considered to be significantly high in the aqueous extract of neem leaves, the theoretical studies have

been performed using these three important phytochemicals.

The proposed mechanistic pathways for formation of G-ZnO NPs are presented in Scheme 1, and associated optimized structures of gallic acid and its derived S1 and S2 are shown in Fig. 10. Formation of $Zn(OH)_2$ from gallic acid, with the possible byproducts (S1 and S2) are validated from the FTIR spectrum in Fig. 2b. The new bands at around $2300 – 2800$ cm^{-1} can be attributed to the C=C–H stretching and C≡C stretching. Moreover, the Ar–COOCH$_3$ groups present in the phytochemicals, as we can see from the structures of nimbin, hydroxyazadiradione etc., can be an excellent intermediate group to form ZnO
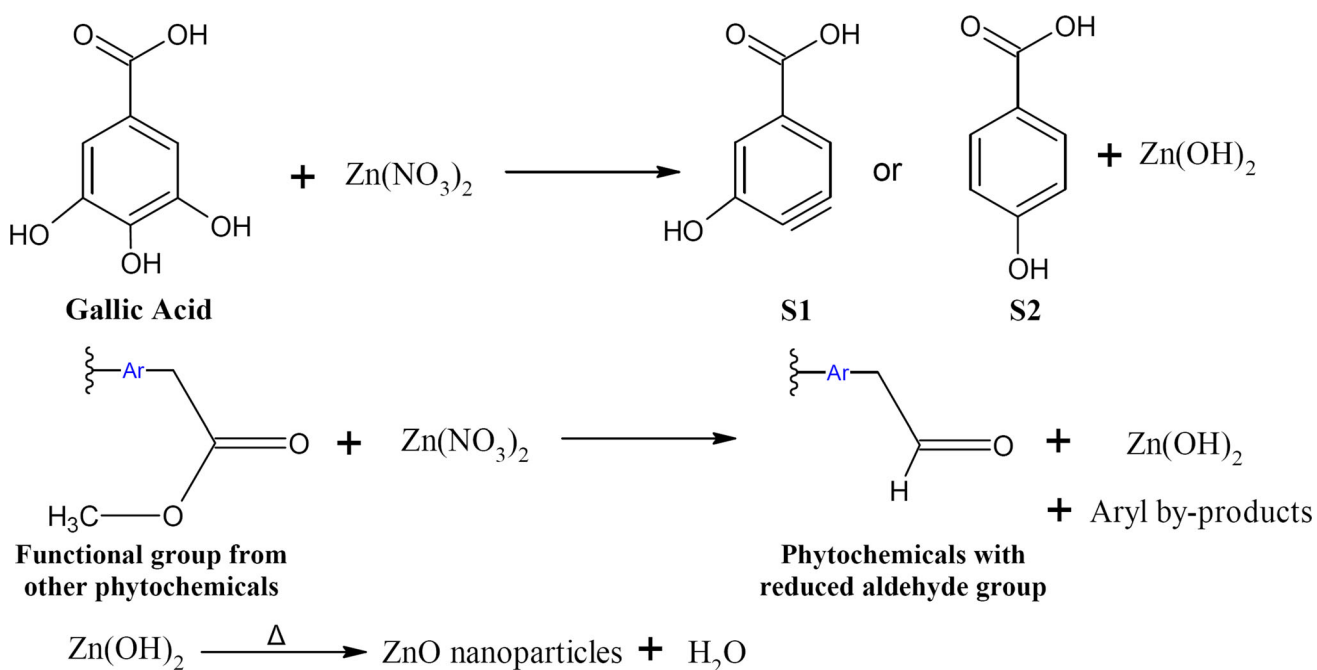
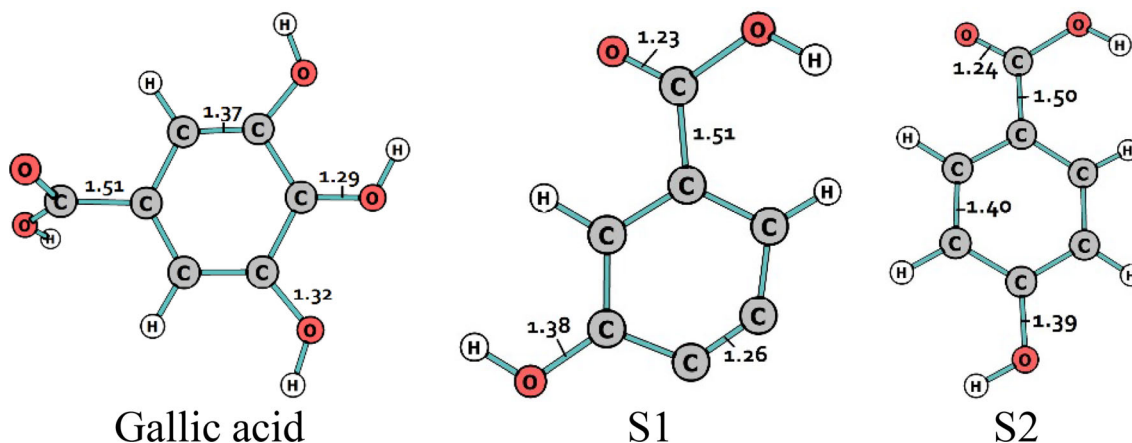Scheme 1 Proposed mechanistic pathways to show the formation of G-ZnO NPs

Fig. 10 Optimized structures of gallic acid and the by-product structures S1 and S2

nanoparticles. The formation of aldehyde Ar–CHO, as expected to be found for these cases, can also be established from the new-found FTIR stretching bands for aldehyde C=O near 1768.78 cm^{-1} and aldehyde C–H near 2880.5 cm^{-1}. Thus, the probable mechanism has lead us to the formation of ZnO nanoparticles via the dehydration of Zn(OH)$_2$.

Concluding Remarks

The present work demonstrates the green synthesis of ZnO nanoparticles (G-ZnO) using *A. indica* leaves extract, where it is well understandable that the green route is much safer and environmentally friendly compared to the chemical synthesis methods. The synthesized G-ZnO nanoparticles were characterized by Fourier transform infrared spectroscopy (FTIR), X-ray diffraction (XRD) technique, Scanning electron microscopy (SEM) images and Energy dispersive X-ray analysis (EDS). The performed characterizations confirmed the presence of the synthesized G-ZnO nanoparticles in an average size of 100–200 nm. The synthesized G-ZnO NPs are found to be in the triangular shape. The larger nanoparticles of G-ZnO are essentially resulted from the agglomeration of smaller nanoparticles due to the electrostatic interactions between the bio-organic capping molecules bound to the G-ZnO nanoparticles and the environmental moisture. Our theoretical investigations incuding the effct of Grimme dispersion correction (DFT-D3) confirm that our synthesized triangular ZnO nanoparticles are better candidate for biological activity in comparison to its conventional spherical counterpart. Overall, synthesized G-ZnO nanoparticles using *A. indica* leaves extract in triangular shape are found to show significant antimicrobial activity against *E. coli* and *B. subtilis* indicating an alternative to the typical chemical methods.

Declarations

Conflict of interest The authors declare that they have no conflict of interest.

References

1. S. S. Joshi, P. R. Patil, M. S. Nimase, and P. P. Bakare (2006). *J. Nanopart. Res.* **8**, 635–643.
2. R. Khan, A. Kaushik, P. R. Solanki, A. A. Ansari, M. K. Pandey, and B. D. Malhotra (2008). *Anal. Chim. Acta* **616**, 207–213.
3. I. Perelshtein, A. Lipovsky, N. Perkas, T. Tzanov, M. Arguirova, M. Leseva, and A. Gedanken (2015). *Ultrasonics Sonochem.* **25**, 82–88.
4. J. A. Barreto, W. O'Malley, M. Kubeil, B. Graham, H. Stephan, and L. Spiccia (2011). *Adv. Mater.* **23**, H18–H40.
5. P. Duran, F. Capel, J. Tartaj, and C. Moure (2002). *Adv. Mater.* **14**, 137–141.
6. C. Bauer, G. Boschloo, E. Mukhtar, and A. Hagfeldt (2001). *J. Phys. Chem. B* **105**, 5585–5588.
7. P. Ramesh, A. Rajendran, and M. Meenakshisundaram (2014). *J. Nanosci. Nanotechnoly.* **2**, 41–45.
8. R. Dobrucka and J. Długaszewska (2016). *Saudi J. Biol. Sci.* **23**, 517–523.
9. B. Li, S. M. Li, J. H. Liu, and M. Yu (2014). *Appl. Surf. Sci.* **315**, 241–246.
10. D. Jain, H. K. Daima, S. Kachhwaha, and S. L. Kothari (2009). *Digest J. Nanomater. Biostruct.* **4**, 557–563.
11. C. B. Ong, L. Y. Ng, and A. W. Mohammad (2018). *Renew. Sustain. Energy Rev.* **81**, 536–551.
12. M. Hasanpoor, M. Aliofkhazraei, and H. Delavari (2015). *Procedia Mater. Sci.* **11**, 320–325.
13. P. K. Samanta and S. Mishra (2013). *Optik-Int. J. Light Electron Opt.* **124**, 2871–2873.
14. M. Laurenti, N. Garino, S. Porro, M. Fontana, and C. Gerbaldi (2015). *J. Alloys Compd.* **640**, 321–326.
15. V. Anand and V. C. Srivastava (2015). *J. Alloys Compd.* **636**, 288–292.
16. A. Šarić, G. Štefanić, G. Dražić, and M. Gotić (2015). *J. Alloys Compd.* **652**, 91–99.
17. S. Ghosh, D. Majumder, A. Sen, and S. Roy (2014). *Mater. Lett.* **130**, 215–217.
18. S. Gunalan, R. Sivaraj, and V. Rajendran (2012). *Progress Nat. Sci.* **22**, 693–700.
19. N. Bala, S. Saha, M. Chakraborty, M. Maiti, S. Das, R. Basu, and P. Nandy (2015). *RSC Adv.* **5**, 4993–5003.
20. D. Gnanasangeetha and D. SaralaThambavani (2013). *Res J Mater Sci* **2320**, 6055.
21. H. A. Salam, R. Sivaraj, and R. Venckatesh (2014). *Mater. Lett.* **131**, 16–18.
22. J. Huang, Q. Li, D. Sun, Y. Lu, Y. Su, X. Yang, H. Wang, Y. Wang, W. Shao, N. He, and J. Hong (2007). *Nanotechnology* **18**, 105104.
23. D. Sharma, M. I. Sabela, S. Kanchi, P. S. Mdluli, G. Singh, T. A. Stenström, and K. Bisetty (2016). *J. Photochem. Photobiol. B* **162**, 199–207.
24. D. Sharma, M. I. Sabela, S. Kanchi, K. Bisetty, A. A. Skelton, and B. Honarparvar (2018). *J. Electroanalyt. Chem.* **808**, 160–172.
25. D. Sharma, S. Kanchi, and K. Bisetty (2019). *Arab. J. Chem.* **12**, 3576–3600.
26. T. R. Lakshmeesha, M. K. Sateesh, B. Daruka Prasad, S. C. Sharma, D. Kavyashree, M. Chandrasekhar, and H. Nagabhushana (2014). *Cryst. Growth Des.* **14**, 4068–4079.
27. A. Belay, M. Mekuria, and G. Adam (2020). *Nanomater. Nanotechnol.* **10**, 1–8.
28. A. Cartwright, K. Jackson, C. Morgan, A. Anderson, and D. W. Britt (2020). *Agronomy* **10**, 1018.
29. K. Varaprasad, G. M. Raghavendra, T. Jayaramudu, and J. Seo (2016). *Carbohydr. Polym.* **135**, 349–355.
30. A. Panáček, M. Kolář, R. Večeřová, R. Prucek, J. Soukupova, V. Kryštof, P. Hamal, R. Zbořil, and L. Kvítek (2009). Antifungal activity of silver nanoparticles against Candidas. *Biomaterials* **30**, 6333–6340.
31. N. Jones, B. Ray, K. T. Ranjit, and A. C. Manna (2008). *FEMS Microbiol. Lett.* **279**, 71–76.

32. J. Chen, J. Zhu, H. H. Cho, K. Cui, F. Li, X. Zhou, J. T. Rogers, S. T. Wong, and X. Huang (2008). *J. Exp. Nanosci.* **3**, 321–328.

33. O. N. Agbenin and P. S. Marley (2006). *J. Plant Protec. Res.* **46**, 215–220.

34. Weast, R.C. (ed.), *Handbook of Chemistry and Physics*, 68th edn. (CRC Press Inc., Boca Raton, FL, 2005) 1987–1988., p. B-144.

35. S. Magaldi, S. Mata-Essayag, C. Hartung de Capriles, C. Perez, M. T. Colella, C. Olaizola, and Y. Ontiveros (2004). *Int. J. Infect. Dis.* **8**, 39–45.

36. C. Valgas, S. M. De Souza, E. F. A. Smânia, I. I. Smânia Jr., and A., (2007). *Braz. J. Microbiol.* **38**, 369–380.

37. R. S. Mondal, D. R. Roy. *Modeling of Bio-Activity and Toxicity in Light of NA Bases Interaction*, (Scholars' Press, Latvia, 2019) European Union.

38. R. G. Parr and W. Yang, *Density Functional Theory of Atoms and Molecules* (Oxford University Press, New York, 1989).

39. M. J. Frisch, et al., *GAUSSIAN 09, Revision D01* (Gaussian Inc, Pittsburgh, 2009).

40. A. D. Becke (1993). *J. Chem. Phys.* **98**, 5648–5652.

41. T. H. Dunning, P. J. Hay, and in: Schaefer III, H.F. (eds.), *Modern Theoretical Chemistry*, vol. 3 (Plenum, New York, 1976).

42. P. J. Hay and W. R. Wadt (1985). *J. Chem. Phys.* **82**, 270–283.

43. S. Grimme, J. Antony, S. Ehrlich, and H. Krieg (2010). *J. Chem. Phys.* **132**, 19.

44. S. Grimme, A. Hansen, J. G. Brandenburg, and C. Bannwarth (2016). *Chem. Rev.* **116**, 5105–5154.

45. R. G. Parr, R. A. Donnelly, M. Levy, and W. E. Palke (1978). *J. Chem. Phys.* **68**, 3801–3807.

46. R. G. Pearson, *Chemical hardness: Applications from molecules to solids* (Wiley, Weinheim, 1997).

47. R. G. Parr, L. V. Szentpaly, and S. Liu (1999). *J. Am. Chem. Soc.* **121**, 1922–1924.

48. R. G. Parr and R. G. Pearson (1983). *J. Am. Chem. Soc.* **105**, 7512–7516.

49. T. Bhuyan, K. Mishra, M. Khanuja, R. Prasad, and A. Varma (2015). *Mater. Sci. Semicond. Process.* **32**, 55–61.

50. S.-H. Nam, T. K. Kim, and J.-H. Boo (2012). *Catal. Today* **185**, 259–262.

51. A. R. Freitas, M. Silva, M. L. Ramos, L. L. Justino, S. M. Fonseca, M. M. Barsan, C. M. Brett, M. R. Silva, and H. D. Burrows (2015). *Dalton Trans.* **44**, 11491–11503.

52. L. Dash, R. Biswas, R. Ghosh, V. Kaur, B. Banerjee, T. Sen, R. A. Patil, Y.-R. Ma, and K. K. Haldar (2020). *J. Photochem. Photobiol. A* **400**, 112682.

53. Z. Chi, L. Zhu, X. Lu, H. Yu, and B. Liu (2012). *Z. Anorg. Allg. Chem.* **638**, 1523–1530.

54. H. Li and Y. Li (2009). *Nanoscale* **1**, 128–132.

55. R. Biswas, A. Kundu, M. Saha, V. Kaur, B. Banerjee, R. S. Dhayal, R. A. Patil, Y.-R. Ma, T. Sen, and K. K. Haldar (2020). *New J. Chem.* **44**, 12256–12265.

56. R. Biswas, S. Mete, M. Mandal, B. Banerjee, H. Singh, I. Ahmed, and K. K. Haldar (2020). *J. Phys. Chem. C* **124**, 3373–3388.

57. P. Rajiv, S. Rajeshwari, and R. Venckatesh (2013). *Spectrochim. Acta A* **112**, 384–387.

58. D. Sharma, J. Rajput, B. S. Kaith, M. Kaur, and S. Sharma (2010). *Thin Solid Films* **519**, 1224–1229.

59. R. Yuvakkumar, J. Suresh, B. Saravanakumar, A. J. Nathanael, S. I. Hong, and V. Rajendran (2015). *Spectrochim. Acta Part A* **137**, 250–258.

60. M. A. Alzohairy (2016). *Evid.-Based Complement. Alternati. Med.* **2016**, 1–11.

61. K. Rangiah, B. A. Varalaxmi, and M. Gowda (2016). *Anal. Methods* **8**, 2020–2031.

62. S. K. Srivastava, B. Agrawal, A. Kumar, and A. Pandey (2020). *J. Sci. Res.* **64**, 385–390.

63. K. S. Santos, A. M. Barbosa, V. Freitas, A. V. C. S. Muniz, M. C. Mendonça, R. C. Calhelha, I. C. F. R. Ferreria, E. Franceschi, F. F. Padilha, M. B. P. P. Oliveira, and C. Dariva (2018). *Pharmaceuticals* **11**, 76–85.

64. S. B. Ulaeto, G. M. Mathew, J. K. Pancrecious, J. B. Nair, T. P. D. Rajan, K. Maiti, and B. C. Pai (2019). *ACS Biomater Sci. Eng.* **6**, 235–245.

65. U. P. Singh, S. Maurya, and D. P. Singh (2005). *J. Herb. Pharmacother.* **5**, 35–43.

66. A. K. Ghimeray, C. W. Jin, B. K. Ghimire, and D. H. Cho (2009). *Afr. J. Biotechnol.* **8**, 3084–3091.

67. K. Sunada, Y. Kikuchi, K. Hashimoto, and A. Fujishima (1998). *Environ. Sci. Technol.* **32** (5), 726–728.

68. M. Fang, J. H. Chen, X. L. Xu, P. H. Yang, and H. F. Hildebrand (2006). *Int. J. Antimicrob. Agents* **27** (6), 513–517.

69. K. Elumalai and S. Velmurugan (2015). *Appl. Surf. Sci.* **345**, 329–336.

70. M. F. Khan, A. H. Ansari, M. Hameedullah, E. Ahmad, F. M. Husain, Q. Zia, U. Baig, M. R. Zaheer, M. M. Alam, A. M. Khan, and Z. A. AlOthman (2016). *Sci. Rep.* **6**, 27689.

71. K. Lingaraju, H. R. Naika, K. Manjunath, R. B. Basavaraj, H. Nagabhushana, G. Nagaraju, and D. Suresh (2016). *Appl. Nanosci.* **6** (5), 703–710.

72. M. F. Elkady, H. H. Shokry, E. E. Hafez, and A. Fouad (2015). *Bioinorg. Chem. Appl.* **2015**, 1–20.

73. M. Banoee, S. Seif, Z. E. Nazari, P. Jafari-Fesharaki, H. R. Shahverdi, A. Moballegh, K. M. Moghaddam, and A. R. Shahverdi (2010). *J. Biomed. Mater. Res. Part B* **93** (2), 557–561.

74. V. Svetlichnyi, A. Shabalina, I. Lapin, D. Goncharova, and A. Nemoykina (2016). *Appl.Surf. Sci.* **372**, 20–29.

75. M. Ramesh, M. Anbuvannan, and G. Viruthagiri (2015). *Spectrochim. Acta Part A* **136**, 864–870.

76. K. Elumalai and S. Velmurugan (2015). *Appl. Sur. Sci.* **345**, 329–336.

77. M. M. Chikkanna, S. E. Neelagund, and K. K. Rajashekarappa (2019). *SN Appl. Sci.* **1**, 117.

78. B. K. Sharma, B. R. Mehta, V. P. Chaudhari, E. V. Shah, S. Mondal Roy, and D. R. Roy (2021). *J Clust Sci.* https://doi.org/10.1007/s10876-021-02090-9.